Ultrathin Pt films on Ni(111): Structure determined by surface x-ray diffraction

O. Robach,[1,*] H. Isérn,[1] P. Steadman,[1,2] K. F. Peters,[1,3] C. Quirós,[1] and S. Ferrer[1]
[1]*European Synchrotron Radiation Facility, BP 220, F-38043 Grenoble, France*
[2]*Diamond Light Source Ltd., Rutherford Appleton Laboratory, Chilton, Didcot, Oxon, United Kingdom OX11 0QX*
[3]*Hewlett Packard, 1000 NE Circle Boulevard, Corvallis, Oregon 97330-4239, USA*
(Received 22 January 2003; revised manuscript received May 27 2003; published 15 December 2003)

The growth of platinum on a nickel (111) single crystal under ultrahigh vacuum conditions was studied using surface x-ray diffraction on the ID03 beamline of the ESRF. Film thickness ranged from one to eight monoatomic layers (ML). Specular reflectivity was used to determine the growth mode and vertical lattice parameter of the Pt film. A two-dimensional (2D) growth up to 1 ML followed by more 3D growth was found. A small expansion of the Pt vertical lattice parameter was found. The Pt in-plane lattice parameter was measured. Its relaxation was found to be very slow, with a residual contraction of 2.3% in an 8-ML-thick film (with respect to bulk Pt). A Ni crystal truncation rod measured before and after growing 1 ML of Pt revealed the presence of a small amount of pseudomorphic Pt, adsorbed on both fcc and hcp sites. The stacking of the (111) Pt planes was investigated by measuring stacking-sensitive Pt diffraction rods. A strong tendency to stacking reversal was found at room temperature, with an amount of ''reversed'' Pt about ten times higher than the amount of Pt with the same stacking as the Ni. An eight-layer Ni film on Pt(111) was also studied for comparison.

DOI: 10.1103/PhysRevB.68.214416 PACS number(s): 68.55.−a, 61.10.−i, 68.35.−p

INTRODUCTION

The Pt-Ni system has recently attracted attention[1–9] due to the perpendicular magnetic anisotropy observed in Pt-Ni multilayers. This property makes this system a potential candidate for high density magnetic recording. From a comparison of Pt-Ni multilayers grown by different methods (dc magnetron sputtering[3,5–9] or *e*-beam evaporation[1,4]), it is clear that the magnetic properties strongly depend on the structure of the films and interfaces that constitute the multilayer. To elucidate the correlation between the magnetic and structural properties, a detailed description of the structure of the Pt-Ni interfaces is needed as a preliminary step.

In this paper, we present a structural study of one of the ''single'' interfaces found in the multilayers, which is the interface obtained by growing Pt on (111) Ni. Our study was done using *in situ* surface X-ray diffraction (SXRD),[10–16] with a Ni(111) single crystal as the substrate. Results are also presented concerning the other ''single'' interface, obtained by growing Ni on Pt(111). These results evidence a strong asymmetry between the two interfaces, in particular regarding the stacking sequence of the (111) Ni planes.

The growth of Pt on a Ni(111) single crystal under ultrahigh vacuum (UHV) conditions has already been the subject of several studies. Barnard *et al.*[17] studied the first stages of the growth at 110–140 K by low energy electron diffraction (LEED) and Auger electron spectroscopy (AES). They also investigated the structures obtained by annealing thin Pt films on Ni(111), by the same techniques,[17] and by photoemission of adsorbed xenon.[18] Deckers *et al.*[19] also studied the growth and annealing using LEED, AES, Rutherford backscattering spectroscopy, and Auger depth profiling. Romeo *et al.*[20] studied the first stages of the growth at room temperature (RT) using photoelectron spectroscopy. The growth of Pt on Ni(111), and the structures obtained by annealing the Pt films, have also given rise to a number of theoretical studies.[21–24] Concerning multilayers, a detailed structural study was published by Staiger *et al.*[25] These authors examined, using high resolution transmission electron microscopy (HRTEM), Pt-Ni multilayers grown by UHV evaporation (2×10^{-10} Torr) on mica substrates covered by a Ru buffer layer.

In this paper, we present experimental results concerning the following points. First we address in detail the morphology of a Pt film grown on a Ni(111) single crystal, giving profiles of the occupation of the different Pt planes, at different stages of the growth.

Second, we examine the question of the strain in the Pt film. We show that the Pt contains a nonpseudomorphic part at all stages of the growth, and we present the evolution of the lattice parameter of this nonpseudo part. We then try to estimate how much of the Pt is pseudomorphic (i.e., with the same in-plane lattice parameter as the Ni). We find, in contrast with a former LEED study, that the amount of pseudomorphic Pt is significantly lower than 1 ML. This may be important for theoreticians who used the existence of a pseudomorphic monolayer as a starting point in their calculations.[23]

Third, we examine the stacking of the (111) planes of the Pt, finding as an interesting result that the dominant stacking in the Pt is the mirror image of the Ni stacking. For the reverse case of a Ni film on Pt(111), in contrast, the dominant stacking in the Ni is the same as for the Pt. This anomaly of stacking, although already noticed by Staiger *et al.*,[25] was never taken into account by theoreticians modeling the Pt-Ni system. An anomaly in the adsorption site (fcc instead of hcp) for Pt adatoms on Ni(111), which could be a ''precursor'' of the stacking reversal, was already predicted theoretically by Castellani *et al.*,[21] but the authors disregarded this result in the rest of their paper. In addition to the potential theoretical interest of trying to understand the origin of the stacking reversal, the taking into account of the

stacking anomaly may be important when trying to predict the magnetic properties of the multilayers. In a previous paper,[26] we proposed that the stacking anomaly may contribute to the perpendicular magnetic anisotropy in Pt-Ni multilayers. The idea was that the change of stacking from one Ni layer to the next creates a sort of ''polytypic'' Ni-Pt alloy, with a hexagonal symmetry and a **c** axis perpendicular to the multilayer stack, and that this **c** axis should be an easy magnetization axis.

Fourth, we examine a surface Pt-Ni alloy obtained by annealing a four-layer Pt film on Ni(111), and deduce an approximate Pt concentration profile near the surface.

Fifth, we discuss our results concerning the strain in the Pt in the light of the theoretical studies. Finally we present the conclusions.

I. EXPERIMENT

The experiments were performed on the ID03 surface diffraction beamline of the ESRF (Grenoble, France), which was previously described in detail.[27] The UHV chamber (base pressure 2×10^{-10} mbar) is mounted on a six-circle diffractometer. It is equipped for sample preparation by sputtering and annealing, for Pt and Ni deposition, and for surface chemical analysis by AES. Two beryllium windows allow the entrance of the incident x-ray beam into the chamber, and the exit of the beam diffracted by the sample. The preparation of the Pt films and the measurements by surface x-ray diffraction were performed *in situ*, under UHV. A commercial Ni(111) single crystal was used (Mateck). It was (111) oriented within $\pm0.1°$. It was prepared by cycles of sputtering at RT and annealing to 750–800 °C. Rocking curve widths were typically 0.04° on the (101) Bragg peak, and 0.3° on the (0 1 0.5) antiphase point of the Ni crystal truncation rod (CTR).[11] Here we describe the reciprocal space using the (H K L) Miller indexes corresponding to the Ni(111) surface unit cell. The lattice vectors of the surface unit cell are $\mathbf{a}_1=\frac{1}{2}[1-10]$, $\mathbf{a}_2=\frac{1}{2}[0-11]$, and $\mathbf{a}_3=[111]$. This gives $a_1=a_2=a_{\mathrm{Ni}}/\sqrt{2}$, and $a_3=\sqrt{3}.a_{\mathrm{Ni}}$ for the lengths where $a_{\mathrm{Ni}}=3.5238$ Å is the bulk lattice parameter of Ni.

The cleanliness of the Ni surface after preparation was checked by Auger electron spectroscopy. The carbon 272-eV and oxygen 510-eV peaks were typically 6% and 3% of the Ni 848-eV peak for our ''clean'' surface. Pt was deposited using an *e*-beam evaporator (Omicron). The depositions rate was calibrated using a quartz microbalance [1 ML Pt(111) = 27 min] and Auger electron spectroscopy (1 ML Pt = 35 min) performed during the growth of Pt on Ni(111). A small oxygen contamination was detected by Auger after the Pt deposition. The Ni sample was either at RT or at 150 K during the Pt deposition. The main study was the growth of Pt on Ni(111). A shorter study was performed for comparison on a 8-ML Ni film deposited at RT on a Pt(111) single crystal. The Pt single crystal was prepared by cycles of sputtering, annealing under vacuum at 800 °C, annealing under 10^{-6}-mbar oxygen at 800 °C to remove the carbon contamination, and short annealing at 1000 °C to desorb the oxygen. Rocking curve widths were typically 0.01° on the (101) Bragg peak, and 0.06° on the (0 1 0.5) Pt CTR point. Ni was deposited using an *e*-beam evaporator (Omicron). The deposition rate was calibrated by estimating the thickness of the Ni film from the out-of-plane width of the Ni(012) Bragg peak [1 ML Ni(111) = 8 min].

The x-ray energy was fixed around the Pt L_{III} absorption edge (11564 eV), except otherwise specified, to allow the simultaneous magnetic characterization by resonant magnetic surface x-ray diffraction.[28–30] The main results of the magnetic study were already presented elsewhere.[26] In the calculation of the structure factors along the diffraction rods, we take into account, when necessary, the reduction of the Pt atomic scattering factor due to the proximity of the Pt L_{III} edge. The values we use for the anomalous corrections are the ones given in Ref. 31, with an averaging to take into account the energy resolution of the monochromator. At the resonance energy, the Pt atomic scattering factor is $f_{\mathrm{Pt}}(q)=f_{\mathrm{Pt0}}(q)-(19.84+8.25\times i)$, where q is the momentum transfer, and $f_{\mathrm{Pt0}}(q)$ is the usual Pt scattering factor, as given in the ROD program,[32–33] and the *International Tables of X-Ray Crystallography*.[34]

For the description of the results, it is important to give more precision on what we call a ''monoatomic layer.'' A first quantity we will use is the ''amount of Pt'' θ, expressed in ML, which is simply the total deposition time divided by the time that it takes to deposit the first layer of Pt (approximately 35 min). When fitting diffraction rods, and giving values of the occupations of the different atomic planes of the Pt film, we will use a more convenient unit, ''Ni-ML.'' One Ni-ML corresponds to the number of atoms per unit of area in a (111) plane of bulk Ni, 1.86×10^{15} atoms/cm^2. The number of atoms per unit area contained in one *complete* atomic plane of Pt, i.e., its surface atomic density, of course depends on the Pt in-plane lattice parameter. In particular, it is not necessarily the same for the top and bottom of the film. For pseudomorphic Pt, i.e., Pt with the same in-plane lattice parameter as Ni, the atomic density is one Ni-ML. For (111)-oriented Pt with the in-plane lattice parameter of bulk Pt, the atomic density will be 0.807 Ni-ML, taking into account the +11.3% lattice mismatch $[=(a_{\mathrm{Pt}}-a_{\mathrm{Ni}})/a_{\mathrm{Ni}}]$ between Pt ($a_{\mathrm{Pt}}=3.9231$ Å) and Ni ($a_{\mathrm{Ni}}=3.5238$ Å).

II. RESULTS

A. Morphology of the Pt films

In this section, we address the morphology of the Pt films grown at RT. From our data, we propose a description of the progressive filling of the different Pt planes during the growth. This is a ''vertical'' description, i.e., we do not have information concerning the lateral morphology (in-plane island size, inter-islands distances). For getting this description, we use measurements of the specular reflectivity at ''high'' angles. This means that the angle of incidence of the x-ray beam with respect to the surface, μ, is above 2°, i.e., much larger than the critical angle for total external reflection. The scattering geometry is with the angle of incidence μ equal to the angle of emergence γ of the diffracted beam with respect to the surface. The incident beam and the

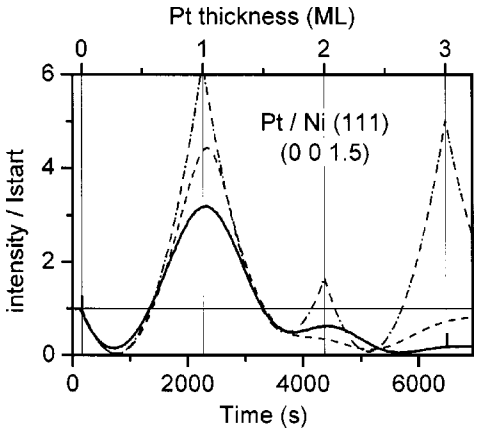

FIG. 1. Evolution of the intensity at the antiphase point on the specular, during Pt deposition on Ni(111) at RT. Solid line: experiment. Dash-dotted line: calculation, perfect layer-by-layer growth. Dashed line: calculation, imperfect growth model.

diffracted beam are in the same plane as the normal to the surface of the sample. A scan increasing μ with $\mu=\gamma$ is the equivalent of the standard θ-2θ reflectivity scan, or of a L-scan along the $(00L)$ rod (also called the specular rod). Such a scan crosses the $(111)_{\text{bulk}}=(003)_{\text{surface}}$ and $(222)_{\text{bulk}}=(006)_{\text{surface}}$ Ni Bragg peaks. The intensity distribution along L in between these Bragg peaks contains information about the vertical profile of electronic density in the sample. This means information about the surface roughness for the clean Ni surface, and about the film thickness, film roughness and Pt perpendicular lattice parameter, for the Pt films on Ni. Some insight into interface roughness and Pt-Ni interfacial distance is also accessible, but only for rather thin films, when a good interference between the Pt scattering and the scattering by the last Ni plane can be obtained.

Here we used two types of measurements. First we monitored the intensity at the anti-phase position (0 0 1.5) during the growth (Fig. 1). This kind of measurement gives growth oscillations, similar to reflection high energy electron diffraction (RHEED) oscillations, due to an alternation of the high surface roughness and low surface roughness, as the successive Pt layers get half-filled then filled. Second, we measured L scans along the $(00L)$ rod for different Pt thicknesses, interrupting the growth during the measurements and restarting it afterwards [Fig. 2(a)]. The L scans were then analyzed using the ROD program[32,33] to find the parameters of the Pt film at the different stages of the growth. This leads, for each Pt thickness θ, to an ensemble of ''XRD occupation rates'' of the different Pt planes, expressed in Ni-ML.

It is important to note that, for each Pt plane, the ''XRD occupation rate'' results from at least three different physical phenomena: first the ''filling'' of the plane (how incomplete it is); second, the degree of strain in the plane (its in-plane lattice parameter); and last but not least, the degree of ''disorder'' of the film. While the effect of the first two phenomena on the diffraction features is simply the same as the effect of an occupation rate, the effect of ''disorder'' is multifold and strongly depends on the type of disorder involved. Highly defective or nonepitaxial regions will just act as ''missing Pt,'' but more subtle forms of disorder, such as

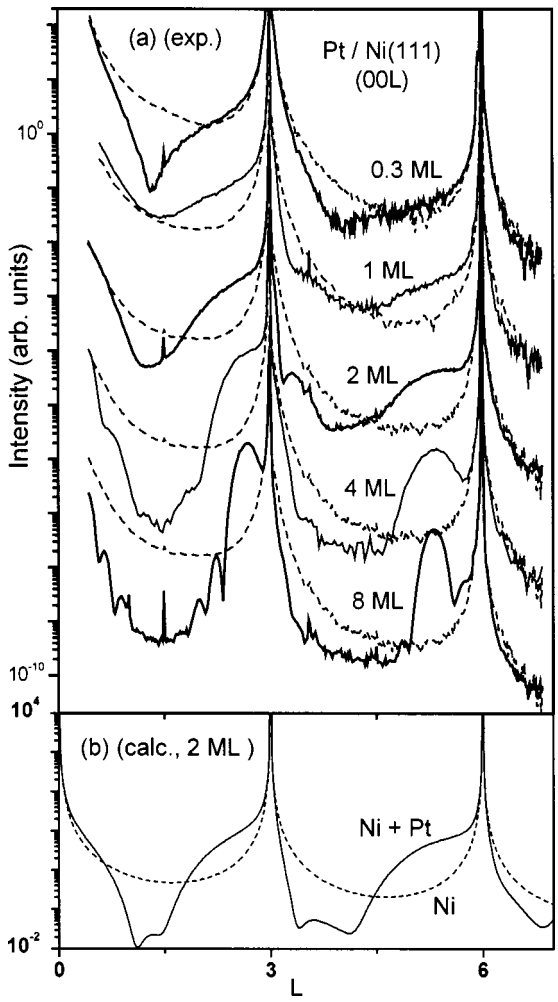

FIG. 2. (a) The specular rod measured at different stages of the growth of Pt on Ni(111) at RT. Dashed lines: clean Ni. Solid lines: Ni+Pt. The Ni Bragg peaks are at $L=0$, 3, and 6. The Pt Bragg peaks build up at $L=0$, 2.7, and 5.4. For large film thickness, thickness fringes are visible around the Pt peaks. (b) Calculation for clean Ni and the ''$\theta=2$ ML'' situation.

variation in the z positions of the Pt planes from one Pt grain to the other, can affect diffraction features very differently depending on whether these features are at high or low diffraction angles. It is out of the scope of this study to enter into this sort of ''disorder analysis'' or into an analysis of the strain distribution in the Pt films. We will limit ourselves to presenting the occupation rates derived from the simplest model: only ''missing Pt''-type disorder, and uniform vertical Pt lattice spacing over the whole film thickness. In practice, all our data on the specular rod lead to a maximum ''XRD occupation rate'' of the Pt planes, equal to 0.6 ± 0.1 Ni-ML. Among the 0.4 ''missing'' Ni-ML, 0.12–0.15 can be accounted for by the lattice parameter on the Pt layer, and 0.25–0.28 we attribute to a ''missing-Pt'' type disorder in the Pt (as a first approximation).

We will first discuss the ''growth curve'' (Fig. 1). The experimental curve (solid line on Fig. 1) is typical of a layer-by-layer growth of the first Pt layer, followed by a less perfect growth of the next layers, as evidenced by the damping

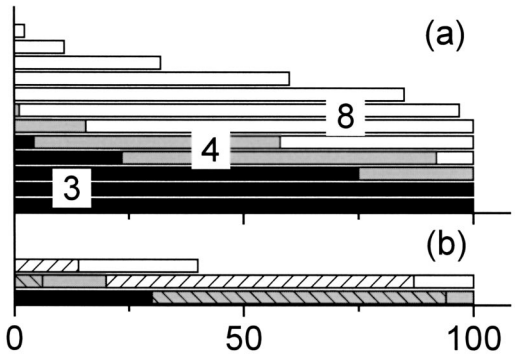

FIG. 3. ''XRD occupation rates'' of the different Pt planes (expressed in percentage of the maximum, 0.6 Ni-ML) at the different stages of the growth, as deduced from the growth curve (Fig. 1) [marked ''(1)''] and from the analysis of the (00*L*) rod (Fig. 2) [marked ''(2)'']. Occupations smaller than 1% are disregarded. (a) White: 8 ML (2); gray: 4 ML (2); black: 3 ML (1). (b). White: 2 ML (2); white+pattern: 2 ML (1); gray: 1 ML (2); gray+pattern: 1 ML (1); black: 0.3 ML (1 and 2).

of the oscillations. For comparison, in Fig. 1 we plot the calculated growth curve for perfect layer-by-layer growth (dot-dashed line). This curve has been calculated with a maximum occupation of each Pt plane of 0.6 Ni-ML. The calculated growth curve shows that the much smaller height of the second maximum, compared to the first maximum, is an interference effect, and not something due to the start of imperfect growth. In contrast, the small height of the third maximum in the experimental curve is clearly a sign of imperfect growth, since this maximum is very high for layer by layer growth. We can therefore say that the transition between layer by layer growth and three-dimensional (3D) growth occurs after the completion of the second Pt layer. A nuance to this statement must be made, since the experimental curve presented variations from one growth to the other, with the second maximum often missing. This means that sometimes the 3D growth starts earlier, before the completion of the second Pt layer. To illustrate the effect of an imperfect layer-by-layer mode on the growth curve, in Fig. 1 we added the calculated growth curve (dashed line) for an empirical growth model where the interlayer transport rate (for atoms descending the steps) is constant and equal to $150/\tau$ up to $t=\tau$ ($\theta=1$ ML), then decreases exponentially to 0 with a time constant of 0.5τ, τ being the time to deposit one Pt layer. This curve is clearly closer to the data than the one of layer-by-layer growth. The ''XRD occupation rates'' of the different Pt planes at $\theta=0.3$, 1, 2, and 3 ML for this model are given in Fig. 3.

We will now discuss the scans along the (00*L*) rod. In Fig. 2(a), we have shown the *L* scans along this rod at $\theta=0.3$, 1, 2, 4, and 8 ML (solid lines), each compared with the *L* scan on the clean Ni. One can follow the buildup and narrowing of the Pt peaks around $L=2.7$ and 5.4, as the Pt lattice forms and the Pt thickness increases. The presence of strong oscillations even at 8 ML indicates that the Pt film stays relatively flat, in spite of the rapid damping of the growth oscillations at the anti-Bragg position during the growth (Fig. 1). The ''XRD occupation rates'' of the different Pt planes deduced from the fitting of the *L* scans are given in Fig. 3. The fit is qualitative, since only line scans were measured, and not rocking scans at each *L*. The visual fitting was done on the following criteria: relative intensities of the rod before and after the deposition of Pt, the position and width of the Pt Bragg peaks, and the number of visible oscillations around the Pt Bragg peaks. Figure 2(b) shows as an example the calculated rods for clean Ni and the ''$\theta=2$ ML'' situation. The fits could be done with zero Ni roughness, meaning that there is no or little interdiffusion at the Pt-Ni interface. The Pt-Ni interfacial distance was fixed at 2.15 Å, which is half the sum of the Pt-Pt and Ni-Ni bulk (111) interplane distances. The Pt-Pt interplane was fixed at the bulk value for low thicknesses, and fitted for larger thicknesses. At $\theta=3$, 4, and 8 ML, it was found to be slightly larger than the value for bulk Pt (100.8%, 100.8%, and 101.2% of the bulk value (2.2650 Å), at 3, 4, and 8 ML, respectively). The shape of the Pt occupation profile, a complementary error function,[32,33,35] was fixed, and its parameters, a thickness and a roughness, were adjusted. As mentioned above, the maximum occupation of each Pt plane was fixed at 0.6 Ni-ML. The ''XRD occupation rates'' in Fig. 3 are given as a percentage of this maximum occupation. From Fig. 3, we can note that the film is almost two dimensional at $\theta=1$ ML (first plane filled, second plane occupied at 20%, third plane empty). At $\theta=8$ ML, 6 of the planes are filled, and the occupation drops to less than 5% between plane 7 and plane 11, meaning a good flatness of the film.

These results compare well with the ones obtained by Barnard *et al.*[17] using AES: these authors also found that the first Pt layer grows in a layer-by-layer mode (at 110–140 K) and that the growth afterwards was less perfect. In fact we also measured the evolution of the main Ni and Pt Auger peaks during the growth, and find results similar to those of Barnard *et al.* There is a clear break in the rise of the Pt (45-eV) peak at $t=35$ min, which corresponds to the completion of the first layer. The time $t=35$ min is also the time needed to reach the first maximum of the x-ray growth curve (Fig. 1). The good flatness of the Pt films and of the Pt-Ni interface that we obtain agrees well with the HRTEM images of Staiger *et al.*[25] These images show that molecular beam epitaxy (MBE)-grown Pt-Ni multilayers on Ru-covered mica present well-defined layers and flat interfaces, except for a ''rippling'' of the multilayer on a lateral scale of 400 Å, associated with a columnar structure, with thinner defective zones between the columns. Another example of good flatness of both Pt and Ni layers in Ni-Pt multilayers MBE grown on glass, is provided by Wilhelm *et al.*[36] They observe, using specular x-ray diffraction, the first-order multilayer satellite peak on a multilayer with Pt and Ni layers as thin as two atomic layers (Ni_2Pt_2). To summarize, our Pt films present a good flatness, at least for the well-oriented part of the Pt. About 25% to 28% of the Pt is disordered, i.e., invisible for diffraction.

B. Strain in the Pt film

In this section, we show results concerning the existence of pseudomorphic Pt (i.e., Pt with the same in-plane lattice

parameter as the Ni) and concerning the evolution of the lattice parameter in the non-pseudomorphic part of the Pt. A very common point of discrepancy between LEED studies and SXRD studies concerning adsorbate growth, is the amount of pseudomorphic adsorbate that can be grown on a given substrate. Except when a LEED *I-V* analysis is performed, the amount of pseudomorphic adsorbate found by LEED observations is usually higher than what is found by SXRD. The reason for this is that the broad and weak peaks due to small domains of nonpseudomorphic adsorbate are very difficult to detect on a LEED screen, especially when they are in the vicinity of intense substrate peaks. One often only sees an increase of the diffuse background of the LEED, and the adsorbate is classified as pseudomorphic, in the absence of contradicting information. In contrast, with SXRD, the large dynamic range available, especially with synchrotron radiation, enables to easily detect the peaks of nonpseudomorphic adsorbate, even in the very first stages of the growth. In addition, with SXRD, the measurement of the substrate's crystal truncation rods (which are analogous to the LEED *I-V* curves except that they are much simpler to calculate) provides a definite way to quantify the real amount of pseudomorphic adsorbate. Thanks to the coherent interference of the scattering from the substrate with the scattering from the pseudomorphic adsorbate, the analysis of the substrate's CTR yields an amount of pseudomorphic adsorbate that is an absolute value, without scaling factor, since the scattering by the substrate serves as an ''internal reference.'' Further discussion about the analysis can be found in Ref. 37. The case of Pt on Ni(111) is a typical example of this discrepancy between LEED and SXRD: Barnard *et al.*[17] announced that the first Pt layer was pseudomorphic, based on visual LEED data. Here we show that in fact nonpseudomorphic Pt appears from the beginning of the growth. We find that there is effectively some pseudomorphic Pt, but that it amounts to less than 0.3 Ni-ML, as will be shown below.

From Barnard *et al.*,[17] Pt is known to grow on Ni(111) with a parallel epitaxy. This means that the Bragg peaks of Pt are going to appear at $(H\ K\ L)$ values which are 0.9 times the $(H\ K\ L)$'s of the Ni Bragg peaks, assuming that the Pt has its bulk lattice parameter. Here we use the term ''nonpseudo Pt'' to designate nonpseudomorphic Pt that grows with the parallel epitaxy (or with the epitaxy deduced from the parallel one by a mirror with respect to the surface, see Sec. II C). The average lattice parameters of this nonpseudo Pt are expected to vary during the growth. In order to detect the nonpseudo Pt, we performed radial in-plane ($L=0.5$) scans along the (-100) direction, such as the one shown in Fig. 4. Here the scattering geometry is with fixed incident angle μ ($\mu=1°$). For a scan at small constant L, such as this one, the angle of emergence γ is almost constant (and small), while the angle θ_S of rotation of the sample around the surface normal, and the angle δ of rotation of the detector around the same axis, vary with approximately $\delta=2\theta_S$. In Fig. 4, which compares the scans before and after deposition of Pt, one can see a sharp peak at $H=-1$, due to the crossing of the Ni $(-10L)$ CTR, and a broad peak around $H=-0.94$, due to the crossing of the Pt rod. This scan, which was performed at $\theta=0.3$ ML, already shows that nonpseudo Pt is present much before the first Pt layer is completed.

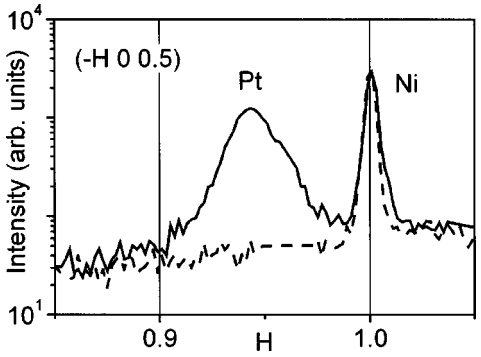

FIG. 4. Radial in-plane diffraction scan around $(HKL)=(-1\ 0\ 0.5)$ showing the sharp Ni CTR at $H=-1$, and the broad Pt rod due to nonpseudo Pt around $H=-0.94$. The vertical line at $H=-0.9$ indicates the expected position for the Pt peak for Pt at its bulk lattice parameter. Dashed line: clean Ni. Solid line: Ni $+0.3$ ML Pt. A clear peak of nonpseudo Pt is already present at $\theta=0.3$ ML.

In order to determine more precisely the moment at which nonpseudo Pt appears, we monitored the intensity of the nonpseudo Pt Bragg peak at $(-0.93\ 0\ 0.9)$ during the growth. The intensity started to rise as soon as the deposition started, meaning that nonpseudo Pt is present from the beginning: there is no stage of ''pure pseudomorphic growth.'' The crystalline quality of the nonpseudo Pt is rather good considering the large lattice mismatch with the Ni: the lateral size of the Pt domains, as derived from the width of the Pt peak along the H scans (such as the one of Fig. 4), varies between 100 and 170 Å. The exact domain size varies slightly with the Pt thickness, but without clear systematic trends: it can either increase or decrease with increasing Pt thickness, depending on the details of the growth (number of growth steps and waiting time between two steps). The in-plane domain size did not change when growing at low temperature (150 K) instead of RT (120 Å for a 4-ML film grown in one step). The mosaic of the Pt is also rather good: the width of the θ_S scan around the Pt peak at $(\approx 0.92\ 0\ 0.5)$ varies between the value expected from the in-plane domain size ($\Delta\theta_S=1.12°$ for $\Delta H=0.018$ and $d=120$ Å) and 0.5° in excess of this value. This means that the Pt mosaic varies between about 0.1° (which is the error bar) and 0.5°, depending on the exact growth conditions.

Concerning now the state of strain of the nonpseudo Pt, a point that is clear from Fig. 4, is that the nonpseudo Pt growing on Ni is far from having reached its bulk lattice parameter: the Bragg peak from nonpseudo Pt should in theory appear at $H=-0.9$, and in practice it appears centered around $H=-0.94$, meaning that the Pt in-plane lattice parameter is intermediate between the value for bulk Ni and the value for bulk Pt. Using H scans analogous to the ones of Fig. 4, performed at different θ's, we measured the evolution of the Pt in-plane lattice parameter during the growth. The results are displayed in Fig. 5. This figure shows that Pt relaxes very slowly towards its bulk lattice parameter: for $\theta=8$ ML, the Pt is still contracted in plane by 2.3%. From

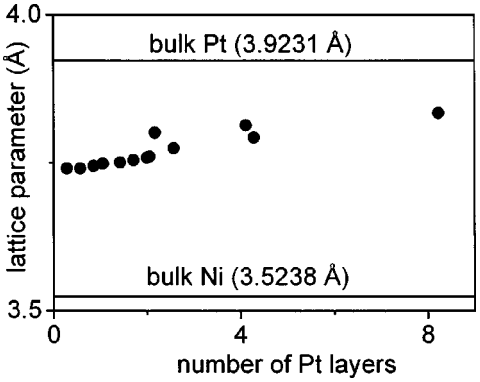

FIG. 5. Evolution of the Pt in-plane lattice parameter during the growth on Ni(111) at RT, for the nonpseudo part of the Pt. Even at $\theta = 8$ ML, the Pt is always contracted with respect to its bulk parameter.

Sec. II A we can remark that this in-plane contraction is accompanied by a small out-of-plane expansion of the Pt lattice parameter (+0.8% at 4 ML, +1.2% at 8 ML). This out-of-plane expansion rules out the possibility that the in-plane contraction would be due to Pt-N alloying. Indeed, alloying would produce an isotropic contraction, i.e., in plane as well as out of plane. The presence of an out-of-plane expansion can be explained by the expected tendency of the Pt unit cell to conserve its the volume during an in-plane expansion induced by the lattice mismatch with the Ni.

It is interesting to note here that the Pt on Ni(111) and the Ni on Pt(111) do not behave at all in the same way from the point of view of strain relaxation. SXRD measurements that we did on an eight-layer Ni film deposited on Pt(111) show that the Ni in-plane lattice parameter is equal to the bulk value. This means that Ni deposited on Pt relaxes much faster towards its bulk lattice parameter than Pt deposited on Ni.

Having discussed the nonpseudo Pt, we now turn to the question of whether there is some pseudomorphic Pt growing simultaneously with the nonpseudo one. In order to answer this question, we measured L scans along a Ni CTR, where an interference between the scattering by the Ni and the scattering by the pseudomorphic Pt is expected to occur, if pseudomorphic Pt is present. Figures 6(a) and 6(c) show a comparison of the Ni $(01L)$ CTR before and after the deposition of 1 (a) and 3(c) ML of Pt. These measurements are again performed in a fixed incidence geometry. On such an L scan, the angle that varies the most is the emergence angle γ of the diffracted beam. The sample rotation θ_S and the detector in-plane rotation δ vary only slightly. One can see that the Pt deposition induces modifications of the Ni CTR. Such modifications can in general be due to several phenomena, and not only to the presence of pseudomorphic Pt. We therefore checked if they could be attributed to one of the two ''straightforward'' causes not involving pseudomorphic Pt which are a relaxation of the Ni surface, and an interdiffusion between Pt and Ni. A relaxation, i.e., a change of the z-position of the last Ni plane, would give an asymmetry of the Ni $(01L)$ CTR around the Bragg peak at $L = 2$, but not change around $L = 0$. As there is a decrease by a factor of 10

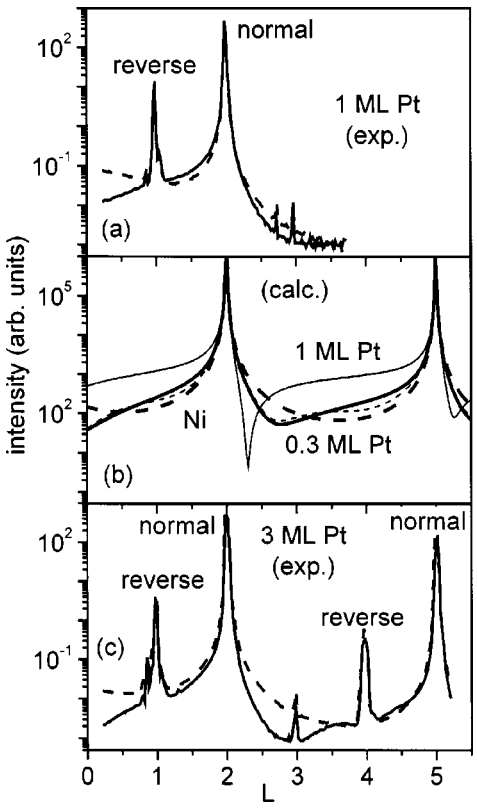

FIG. 6. (a) and (c) Comparison between the Ni $(01L)$ CTR before (dashed lines) and after (solid line) the deposition of Pt, showing the presence of pseudomorphic Pt, in the Pt growing on Ni(111) at RT. (a) is at 11.5 KeV, (c) at 17 KeV, allowing a larger L range. A few ''unexpected'' peaks are present: the ones at $L = 1$ and 4 are due to imperfections of the bulk Ni (domains with a reversed stacking of the (111) planes; see Sec. II C). The one at $L = 3$ is a harmonic of the (039) Bragg peak. (b) shows the calculated rod: Ni only (thick dashed line), Ni + 0.3 Ni-ML 2D pseudomorphic Pt (thick solid line), Ni + 1 Ni-ML 2D pseudomorphic Pt (thin solid line), Ni + 0.26 Ni-ML 3D pseudomorphic Pt (thin dashed line). We assumed a 50%-50% mixture of fcc and hcp sites for the calculation. The amount of pseudomorphic Pt is clearly lower than 1 Ni-ML.

of the intensity around $L = 0$ in the data [see Fig. 6(a)], it is clear that a relaxation of the Ni is not sufficient to describe the modifications. An interdiffusion would have, in a first approximation, the same effect on the Ni CTR as an increase of roughness, meaning a general decrease of the Ni CTR, with the largest decrease at the ''anti-Bragg'' positions. Since the data show an increase of the intensity near $L = 1.5$, an interdiffusion alone is not sufficient either to describe the modifications. Combining a 0.12-Å outward relaxation of the last Ni plane and a 10% decrease of occupation of the last Ni plane (to mimic the interdiffusion) gives the right tendencies, but not the right shape around $L = 0$. Unless the Pt deposition induces a rather complicated modification of the Ni surface, it therefore seems reasonable to propose that there is some pseudomorphic Pt. Anomalous scattering measurements near the Pt edge on the Ni CTR would be a definitive check for this.

From now on, we make the hypothesis that the modifications of the Ni CTR do come from pseudomorphic Pt. Con-

cerning the amount of pseudomorphic Pt, one can say that the relative weakness of the modifications of the Ni CTRs is rather misleading. At first thought, given the much larger number of electrons of Pt compared to Ni, one would expect to get a large increase of the Ni CTR, even for small amounts of pseudomorphic Pt. With this kind of reasoning, we would say that, from our data, the amount of pseudomorphic Pt must be almost negligible, less than 0.1 ML. At second thought, however, it appears that this interpretation holds only if all the Pt atoms sit on fcc sites of the Ni surface. If the Pt atoms are allowed to occupy indifferently fcc or hcp sites, the interference effect due to Pt on the Ni CTRs will be much smaller. This is because the scattering from Pt atoms on fcc sites interferes coherently with the one of Pt atoms on hcp sites, and there is a large phase shift between these two scatterings (at least on this particular CTR), so that the interference is mostly destructive. In other words, we can say that the presence of a mixture of fcc and hcp sites in the first Pt plane tends to destroy the interference between Pt and Ni on the Ni CTRs. This is true of course only for CTRs like the $(01L)$, which are sensitive to the stacking of the $(111)_{\mathrm{bulk}}$ planes: the $(11L)$ rod would be insensitive to this effect.[38–40]

Our data here are too limited to attempt a determination of how much of the pseudomorphic Pt sits on the fcc sites, and how much sits on the hcp sites. What one can say is that the ''single-site'' models (100% fcc site or 100% hcp site) do not fit the data properly: a mixture of the two sites is necessary. Here we will consider for the calculations only the case with a 50%–50% mixture of fcc and hcp sites. This case corresponds to a maximum of destructive interference between the scattering from the two sites, i.e., the effect produced on the Ni CTR by a given amount of pseudomorphic Pt is the lowest. This means that the amount of pseudomorphic Pt deduced from comparing these calculations with the data will be an ''upper limit'' of the real amount. Figure 6(b) shows the calculated Ni $(01L)$ CTR for three different situations: clean bulk terminated Ni (dashed line), the same after adding 0.3 Ni-ML of Pt (thick solid line), and the same with a total of 1 Ni-ML (thin solid line). In the calculation the Pt is pseudomorphic and occupies only one plane. The Ni roughness is zero, and the Pt-Ni interfacial distance is 2.15 Å. The qualitative comparison between Figs. 6(a) and 6(b) shows that our data at $\theta=1$ ML are well reproduced with the model containing 0.3 Ni-ML of pseudomorphic Pt, and that the model with 1 Ni-ML of pseudomorphic Pt does not fit at all. We therefore conclude that, for $\theta=1$ ML, the amount of pseudomorphic Pt in the film is less than 0.3 Ni-ML. Given the fact that about 25–28 % of the Pt film are ''invisible'' for diffraction, due to disorder (as mentioned in Sec. II A), the amount of pseudomorphic Pt may not be so negligible after all: at $\theta=1$ ML, pseudomorphic Pt may represent up to 45% of the ''ordered'' Pt. It should be noted that the assumption of 2D Pt, that we made for the calculation, is not necessary to obtain a shape of the Ni CTR similar to the experimental one: 3D Pt also works. As an illustration, the thin dashed line in Fig. 6(b) shows the calculated CTR for ''3D'' pseudomorphic Pt. Here two Pt planes are occupied, with occupations of 0.2 and 0.06 Ni-ML. The Pt-Pt interplane distance is 2.265 Å. The structure is a 50%–50% mixture of ''fcc site + normal stacking'' and ''hcp site + reversed stacking'' (see Sec. II C).

We can get some insight on what happens to the pseudomorphic Pt after $\theta=1$ ML by comparing Figs. 6(a) and 6(c). The Ni CTR continues to evolve between $\theta=1$ and 3 ML, indicating that pseudomorphic Pt continues to grow. The fact that the Ni CTR passes below the one for clean Ni on both sides of the Bragg peak at $L=2$ indicates that the pseudomorphic Pt becomes more ''3D.'' Here we do not have the data (typically a continuous monitoring of the Ni CTR intensity during the growth) that would allow to say exactly when the pseudomorphic Pt stops growing.

C. Stacking of the (111) planes in the Pt

In this section, we will show that the dominant stacking in the Pt is reversed compared to the Ni stacking, when growing Pt on Ni(111). We will also show that this is not true when growing Ni on Pt(111): here the dominant stacking in the Ni film is the same as in the Pt substrate. From the point of view of the stacking of the (111) planes, our Ni(111) single crystal contains two twins: a dominant one, which we call ''normal,'' that has an *ABCABC*... stacking of the (111) planes along the [111] direction; and a minority one, which we call ''reversed'' or ''twin,'' which has an *ACBACB*... stacking. The dominant twin is also the one present at the surface, as shown by the fact that the Ni CTR signal originates from the Bragg peaks of the ''normal'' twin. The ''reversed'' twin is more bulklike and does not give rise to measurable CTRs, so we can consider that it does not exist at the surface. Pt adatoms that arrive on the Ni surface of the ''normal'' Ni can *a priori* occupy two types of sites: fcc sites, which continue the *ABC* stacking of the Ni, or hcp sites, which represent a fault compared to the Ni stacking. If the Ni is terminated by a ''*C*'' plane, Pt on a fcc site would be in an ''*A*'' plane, while Pt on a hcp site would be on a ''*B*'' plane. When Pt starts to grow as a film with several layers, its (111) planes can adopt either a ''normal'' stacking or a ''reversed'' stacking. This possibility for two twins (normal or reversed) prevents in general the film from being as ''single crystalline'' as the substrate, even in the case of homoepitaxial growth. Thanks to the large penetration depth of x rays, SXRD can easily bring information about this stacking of the Pt(111) planes. The way to obtain this information is by measuring a L scan along a rod of the Pt film, taking care to choose a rod that is sensitive to the stacking, such as the $(-0.92\ 0\ L)$. Along such a rod, the Bragg peaks of Pt with the ''normal'' stacking are at different L positions than the ones of Pt with the ''reversed'' stacking, so that distinction between the two stackings is easy. Of course, the Pt needs to contain at least three planes to make this analysis.

Figure 7(a) shows two L scans. The first one is along the Ni $(-10L)$ CTR, measured on the clean Ni before the deposition. The second one is along the neighboring $(-0.92\ 0\ L)$ Pt rod, measured for an eight-layer-thick Pt film. On the Ni CTR, the Bragg peaks appear at $L=2$ and 5 for the ''normal'' stacking, and at $L=1$ and 4 for the ''reversed'' stacking. On the Pt rod, due to the larger lattice

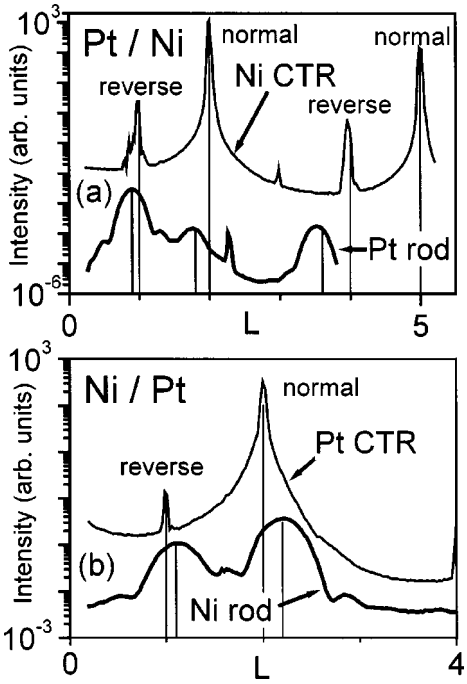

FIG. 7. Comparison between a Ni rod, and the neighboring Pt rod. (a) For Pt on Ni(111). The dominant stacking in the Pt film is reversed compared to the stacking of the Ni substrate. (b) For the reverse growth of Ni on Pt(111). Here the dominant stacking in the Ni film is the same as in the Pt substrate.

parameter, the Pt Bragg peaks are expected at $L=1.8$ and 4.5 for the ''normal'' stacking, and at $L=0.9$ and 3.6 for the ''reversed'' stacking. One can see on this rod that the two stackings are present in the Pt, with a large predominance of the ''reversed'' stacking. This predominance of the ''reversed'' Pt is quite large in Pt films grown at RT, but decreases in Pt films grown at low temperature. For example, for a 4-ML-thick Pt film, the ratio between the intensities of the peaks at $L=0.9$ and 1.8 is about 12 at 300 K, and decrease to 4 at 150 K. This may be an indication that the Pt with ''reversed'' stacking is more stable, thermodynamically speaking, than the Pt with the normal stacking. In order to estimate the respective proportions of the two twins, we performed quantitative measurements of the Pt $(0.93L-0.93L)$ rod (i.e., θ_S scans at several L's instead of a L scan). This was done for the 4-ML-thick Pt film grown at 150 K. The analysis of this rod gave 74% of ''reversed'' stacking and 26% of ''normal'' stacking. The ratio reversed/normal is therefore about 3:1 at 150 K, and about 9:1 at 300 K.

For comparison, we also performed the same type of measurements on the reverse system of Ni on Pt(111). We analyzed the stacking of a 8-ML-thick Ni film grown at RT on a Pt(111) single crystal. The results are presented in Fig. 7(b), with an L scan along the $(01L)$ CTR of the Pt substrate, and an L scan along the neighboring rod of the Ni film at $(0\ 1.1\ L)$. Both scans were performed after the deposition. This time we use the Pt lattice as a reference for (HKL). The Bragg peak for ''normal'' Pt being at $L=2$ on the CTR, we expect, on the Ni rod, Bragg peaks at $L=2.2$ for the ''normal'' stacking, and at $L=1.1$ for the ''reversed'' stacking. One can see on the Ni rod that the two stackings are present in the Ni film, but this time with the ''normal'' stacking dominating. The intensity ratio between the peaks at $L=2.2$ and 1.1 is about 3.5. The tendency for stacking reversal observed when growing Pt on Ni(111) is therefore not present when growing Ni on Pt(111).

This stacking anomaly was already pointed out by Staiger *et al.*[25] in the course of studying Pt-Ni multilayers using HR-TEM in a side view. These authors noted that the probability for stacking reversal was high when growing Pt on Ni, and almost zero when growing Ni on Pt. The origin of the stacking reversal of Pt on Ni is not known. In particular, it is not clear if this is a kinetic effect (due to the details of the growth process, such as the shapes of the monolayer islands) or a thermodynamic effect. Calculations of the energy of three-layer Pt films on Ni(111) with different stackings would be needed to determine it this is a thermodynamic effect. Comparative simulations of the Pt on Ni and Ni on Pt cases would also be useful. In the case of Ni on Pt at RT, we in fact already have an indication that the difference of energy between the normal and reversed stackings may be rather small. Indeed, the predominance of the normal stacking over the reverse stacking can be reverted by simply preadsorbing CO on the Pt(111) surface before the growth [the peak ratio $I(2.2)/I(1.1)$ changes from 3:1 to 1:1.6].

A first step toward the explanation of the stacking reversal may be the theoretical study of Castellani *et al.*[21] These authors calculated the energy of single Pt adatoms adsorbed on different sites of the Ni(111) surface. They found that hcp sites are significantly more favorable than fcc sites (by 0.13 eV/atom). However, they apparently did not consider this result as very significant, since in all following simulations they assumed that Pt atoms were adsorbed on fcc sites. Experimentally, there is some agreement with the theoretical expectation for a hcp site. Our data on the Ni CTR indicate that some of the pseudomorphic Pt is adsorbed on the hcp sites, although not all of it. This result goes in the right direction, although, as mentioned above, it concerns only the small portion of the Pt that is pseudomorphic, not all the Pt. Staiger *et al.*[25] mention that ''the twinning is rarely observed inside the layers... but occurs predominantly at an interface Pt/Ni.'' This would mean that their Pt films consist of ''single-twin'' columns, i.e., when Pt starts growing with a certain stacking (normal or reversed) over a certain area, it keeps this same stacking later on. This is consistent with our diffraction measurements, which show that the two twins have the same out-of-plane domain sizes, and that this domain size is equal to the film thickness. The last part of Staiger's statement seems to indicate that, for columns growing with the reversed stacking, the fault occurs in the first Pt plane, i.e., the Pt is adsorbed on a hcp site. This would agree with the findings of Castellani *et al.*

Finally, we can also remark that the preference of adatoms for the hcp site is not so uncommon, since molecular dynamics simulations predict that it should also happen for Co adatoms on Au(111).[41] From the point of view of stacking, the case of Co $(0001)_{\mathrm{hcp}}$ or $(111)_{\mathrm{fcc}}$ oriented layers presents the additional complication that Co can form under two phases, the hcp one, which is the most stable at RT in bulk Co, and

the fcc one. This is in contrast with Ni, which rarely forms polytypes, except for example in the growth on Ag(100), where a $4H$ phase is observed.[42,43] The stacking of Co in $(0001)_{hcp}$ layers has been studied extensively, but most authors focused on the fcc or hcp character of the Co, and not on the relative proportions of the two twins in the fcc Co. This is probably due to the difficulty of stabilizing well-ordered fcc Co layers, especially in the form of single layers, which are the most convenient for SXRD studies. For example, in the Co-Cu(111) system, well-ordered fcc Co layers up to 65 Å thick[44–46] can be obtained in Co-Cu(111) multilayers (grown at 50 °C), but on a Cu(111) single crystal, 4-ML-thick Co films (grown at RT) already start switching to hcp.[47,48] Studying the reverse growth of Cu(111) films on a single-twin fcc Co(111) surface is also complicated, due to the unavailability of good fcc Co single crystals. In spite of these difficulties, one can already start to discuss the relative proportions of the two twins in the fcc Co-Cu(111) system, based on existing studies of Co-Cu multilayers. From the data of Lamelas *et al.*[44] and Boedeker *et al.*[45] taken on Co-Cu multilayers with $t\mathrm{Co}<40$ Å, one can first remark that at least one of the growths (either Co on Cu or Cu on Co) occurs with stacking conservation, since the coherence thickness for the fcc stacking [as deduced from the $(10L)$ hcp diffraction rod] is approximately equal to the thickness of a Co-Cu bilayer. Second, there is an indication that the other growth occurs with either a stacking reversal (twin fault[39]) or at least one deformation fault[39] at the interface, since the ''stacking independent'' coherence thickness [as deduced from the $(00L)$ diffraction rod] is much larger (about ten bilayers). Further studies would be needed to clarify this point, but this already gives a hint that the anomalous stacking behavior observed in Pt-Ni may also exist in other systems.

D. Surface alloying

In this section, we examine a surface Pt-Ni alloy obtained by annealing a Pt film deposited on Ni(111). Our sample was prepared by growing 4 ML of Pt on Ni(111) at 150 K, then annealing shortly at 470 °C. Pt and Ni are fully miscible in the solid phase, and present three compound phases, Pt_3Ni, PtNi, and $PtNi_3$, which can be ordered into $L1_0$ and $L1_2$ phases by appropriate treatments.[49,50] When annealing a Pt layer deposited on Ni(111), two competing tendencies come into play: the tendency of the Pt to dissolve into the Ni to form an alloy, and its tendency to segregate to the surface.[23,24] The tendency of the Pt to surface segregation is observed in particular at the surface of bulk Pt-Ni alloys.[51] Gauthier[51] proposed, using *I-V* LEED, a description of the concentration profile near the low index surfaces of various bulk Pt-Ni alloys. For a $Pt_{50}Ni_{50}(111)$ alloy, the Pt concentrations in the last alloy planes are $C_1=88\%$ (Pt enrichment in the topmost plane), $C_2=9\%$ (Pt depletion in the next plane), and $C_3=65\%$ (small Pt enrichment in the third plane). Gauthier designs this alternation of Pt enrichment ($C>C_{\mathrm{alloy}}$) and Pt depletion ($C<C_{\mathrm{alloy}}$) as a ''concentration oscillation.''

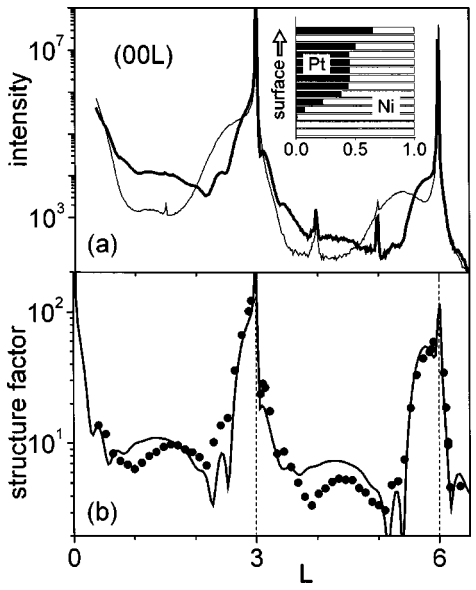

FIG. 8. (a) L scans along the specular rod, before (thin line) and after (thick line) annealing a four-layer Pt film on Ni(111). The Pt film transforms into a thicker subsurface Pt-Ni alloy. (b) Experimental structure factors (points) along the specular rod, for the surface alloy, compared to the calculated rod (line), for the Pt concentration profile shown in the inset. The structure factors are obtained by measuring one rocking scan of the sample (μscan at constant $\mu+\gamma$) at each L.

In our sample, the effect of the annealing on the diffraction features is the following. First the H position of the ''Pt'' peak on an in-plane scan similar to the one of Fig. 4, shifts from $H=-0.92$ to about -0.94. This shift corresponds to the incorporation of Ni into the Pt, which makes the ''Pt'' lattice parameter decrease. We can note here that our surface alloy is not pseudomorphic with the Ni substrate, in contrast with the assumption taken by Legaré *et al.*[24] for their calculations. Another effect of the annealing is a strong decrease of the Ni CTR at (1–1 0.5), which indicates that the interface between the Ni and the surface alloy is rougher compared to the interface between Ni and the as-deposited Pt. The effect of the annealing on the $(00L)$ specular rod is shown in Fig. 8(a), which compares the L scans along this rod before (thin line) and after (thick line) annealing. One can see that the ''Pt'' Bragg peaks at $L=2.7$ and 5.4 shift toward the neighboring Ni Bragg peaks at $L=3$ and 6. This indicates a contraction of the vertical lattice parameter, associated with the incorporation of Ni into the Pt. The ''Pt'' peaks also narrow, and the period of the thickness fringes around these Bragg peaks decreases. This indicates that the alloy layer is significantly thicker than the original Pt layer. Another characteristic feature, on the L scan after annealing, is the oscillation of large period near $L=1.5$ and 4.5. This oscillation is the signature of the presence of a ''modified'' layer with a thickness of 2–3 planes. Such an oscillation can not be obtained from ''monotonous'' Pt concentration profiles, such as the one due to a diffuse interface between the alloy and the bulk Ni, or the one due to a simple surface segregation of the Pt. It can however be reproduced using a model similar to the one of Gauthier,[51] with a Pt enrichment in the last plane, and a Pt

depletion in the next plane. In Fig. 8(b), we show, as an example, a comparison between the data on the $(00L)$ rod for the alloy and the calculated rod using the concentration profile shown in the inset. In the calculation, the distance between two successive planes is obtained applying Vegard's law $[d_{111}(\mathrm{Pt}_x\mathrm{Ni}_{1-x}) = x.d_{\text{Pt-bulk}} + (1-x).d_{\text{Ni-bulk}}]$, taking into account the Pt concentrations in both planes.

The main features of our concentration profile are consistent with the ones obtained by Deckers *et al.*,[19] using Auger depth profiling, after annealing a 5.5-ML Pt film at 450 °C for 30 h. As in the study of Deckers *et al.*, the Pt does not dissolve completely into the Ni, but forms a surface alloy with a well defined thickness. The alloy concentration is 35–45 % in our case, compared to 50% for Deckers *et al.*, and the alloy presents a concentration oscillation at the surface.

III. DISCUSSION

It is interesting to discuss our results concerning the strain in the Pt in the light of the theoretical studies performed on the Pt/Ni(111) system by Castellani and co-workers[21,22] and Legaré *et al.*[23,24] From our data, we find that pseudomorphic Pt may be present, and amounts to up to 0.3 Ni-ML at $\theta = 1$ ML. The presence of pseudomorphic Pt is rather surprising, since the lattice mismatch between Pt and Ni is large (+11.3%), but in fact this result is supported by a theoretical study.[23] Legaré *et al.* find that a Ni(111) surface covered by one layer of pseudomorphic Pt is surprisingly very stable, more stable that either the clean Pt(111) surface or the clean Ni(111) surface. They explain this fact by the following arguments. First, at the Pt(111) surface, broken bonds lead to a tensile[52] surface stress, which tends to a reduction of the lattice parameter in small Pt particles. The in-plane compression that the Pt layer undergoes when it is adsorbed pseudomorphically on Ni(111) therefore helps it to be more stable. In particular, it becomes more stable than the last Pt layer of a Pt crystal, which is forced by the underlying Pt to keep, at least in plane, the bulk lattice parameter. Second, the pseudomorphic Pt monolayer on Ni(111) is stabilized by the chemical affinity between the two metals in contact. Where our study contradicts the one of Legaré *et al.*[23] is in the amount of pseudomorphic Pt, which is lower in our case (0.3 Ni-ML instead of 1 Ni-ML). This discrepancy between theory and experiment is probably due to the fact that lateral relaxations of the Pt may lower the calculated energy, and were not taken into account in Ref. 23.

We will now discuss the very slow relaxation that we observed for the nonpseudo Pt. At $\theta = 8$ ML, we find that the in-plane lattice parameter of the nonpseudo Pt is still contracted by 2.3%. We could argue that the tensile stress at the surface of the Pt film would help to maintain the Pt film in a contracted state over a large thickness range, but this does not seem a good argument. Indeed the Pt tensile stress should, at least near the surface, induce an isotropic contraction of the Pt unit cell, not the combination of in-plane contraction and out-of-plane expansion that we observe. Therefore, the slow relaxation that we observe for the in-plane Pt lattice parameter seems to be dominantly the result of the deformation induced by the lattice mismatch with the Ni, and the role of the Pt tensile stress seems secondary. We can note that, for the reverse system of Ni on Pt(111), the tensile surface stress of the Ni (Refs. 52 and 53) will tend to decrease the Ni in-plane lattice parameter, while the lattice mismatch with the Pt will tend to increase it. In this case the two phenomena have opposite effects, while they had concurring effects in the case of Pt on Ni. This may explain why the strain relaxation is much faster for Ni on Pt than for Pt on Ni(111).

An important point to note is that the deposition process itself may be the source of the film stress (and strain), independently of any problem of lattice mismatch. In the course of characterizing their Pt-Ni multilayers by *in situ* stress measurements during the growth, Kim *et al.*[5] found that a pure Ni film was under tensile stress, while a pure Pt film was under compressive stress. If a ''process derived'' compressive stress also exists in our Pt layers, this process stress may play a role in the slow relaxation that we observe for Pt films on Ni(111). Of course it is not clear if our UHV evaporated films will present intrinsic stresses of the same sign as the films of Kim *et al.*,[5] which are deposited by dc magnetron sputtering. In situ stress measurements in the case of UHV evaporation would be needed in order to clarify this. Such ''process derived'' stress is difficult to model theoretically, since it involves taking into account the deposition process. The complexity of the problem is well illustrated by a remark by Kim *et al.*,[5] that the process stress in their Ni layers can be changed from tensile to compressive just by varying the Ar sputtering pressure from 7 to 1 mTorr.

Another theoretical study, which we can try to compare our results with, is the study by Castellani *et al.* on small Pt aggregates adsorbed on Ni(111).[21] Castellani *et al.* modeled Pt clusters containing at most four atoms, adsorbed in various geometries (linear, planar losange, tetrahedron) on Ni(111). In contrast with the study of Legaré *et al.*,[23] which involved only pseudomorphic Pt, Castellani *et al.* allowed for lateral displacements of the Pt atoms. Of course due to the very small size (four atoms) of the simulated aggregates, we can only compare the theoretical results with our data at the lowest coverage studied, which is 0.3 ML. For this coverage, the island size is 120 Å or more (one island can contain several domains), and we found an in-plane lattice parameter of the Pt of 3.74 Å (Fig. 5), meaning a nearest-neighbor Pt-Pt distance of 2.64 Å, which is 95.3% of the bulk value. The calculation of Castellani *et al.* gives in-plane Pt-Pt distances of 97.6% of the calculated bulk value (2.772 Å) for a Pt dimer, 102.4% for a triangular planar Pt trimer, and 99% for the planar losange Pt tetramer. All these calculated Pt-Pt distances are larger than our experimental value (95.3%) but they reproduce the experimental tendency that, even for Pt in a 2D form, a part of the Pt relaxes towards the Pt bulk lattice parameter. It is difficult to push further the comparison between the calculated and experimental values, since other configurations of the clusters give Pt-Pt distances smaller than the experimental value. This is the case for example for the linear trimer (93.3%), and for the linear tetramer (91.8%). As we already mentioned, in the modeling of the clusters, Castellani *et al.* considered only Pt atoms adsorbed on fcc sites, disregarding the preferential hcp site they

found for monoatomic adsorption. We can wonder if changing the adsorption site would influence the Pt-Pt interatomic distance that they find.

IV. CONCLUSION

We have studied the morphology and strain of thin Pt films deposited on Ni(111). The growth mode found here (2D growth for the first layer, then more 3D growth) agrees well with the experimental results published in the literature. We find that there may be some pseudomorphic Pt, as predicted by a theoretical study, but the amount of pseudomorphic Pt that we find (at most 0.3 Ni-ML at $\theta=1$ ML) is lower than the one expected by theory, and found in a LEED study. For the nonpseudo Pt, which appears as soon as the deposition starts, we find a very slow relaxation of the Pt in-plane lattice parameter toward the bulk value, which is not complete even at $\theta=8$ ML. Concerning the stacking of the (111) Pt planes, we find that the dominant stacking in the Pt is the mirror image of the Ni stacking. This result may be correlated with the theoretical expectation that hcp sites are more favorable than fcc sites for Pt adatoms on a Ni(111) surface. A surface Pt-Ni alloy obtained by annealing a Pt film was also studied. The Pt concentration profile across the alloy layer is in good agreement with the general tendencies obtained by other authors.

*Corresponding author. Email address: robach@esrf.fr. Fax: (+33) 4 76 88 21 60.

[1] M. Angelakaris, P. Poulopoulos, N. Vouroutzis, M. Nyvlt, V. Prosser, S. Visnovsky, R. Krishnan, and N. K. Flevaris, J. Appl. Phys. **82**, 5640 (1997).
[2] R. Krishnan, H. Lassri, M. Porte, M. Tessier, and P. Renaudin, Appl. Phys. Lett. **59**, 3649 (1991).
[3] S. C. Shin, G. Srinivas, Y. S. Kim, and M. G. Kim, Appl. Phys. Lett. **73**, 393 (1998).
[4] F. Wilhelm, Ph.D. thesis, dissertation.de Berlin, 2000.
[5] Y. S. Kim and S. C. Shin, J. Magn. Magn. Mater. **198–199**, 602 (1999).
[6] Y. S. Kim and S. C. Shin, Phys. Rev. B **59**, R6597 (1999).
[7] Y. S. Kim and S. C. Shin, IEEE Trans. Magn. **34**, 858 (1998).
[8] G. Srinivas and S. C. Shin, J. Magn. Magn. Mater. **198–199**, 341 (1999).
[9] S. K. Kim, J. R. Jeong, J. B. Kortright, and S. C. Shin, Phys. Rev. B **64**, 052406 (2001).
[10] I. K. Robinson and D. J. Tweet, Rep. Prog. Phys. **55**, 599 (1992).
[11] I. K. Robinson, Phys. Rev. B **33**, 3830 (1986).
[12] I. K. Robinson, R. T. Tung, and R. Feidenhans'l, Phys. Rev. B **38**, 3632 (1988).
[13] S. R. Andrews and R. A. Cowley, J. Phys. C **18**, 6247 (1985).
[14] G. Renaud, J. Phys. III **4**, 69 (1994).
[15] E. Vlieg, J. F. van de Veen, S. J. Gurman, C. Norris, and J. E. Macdonald, Surf. Sci. **210**, 301 (1989).
[16] S. Ferrer, Surf. Sci. Lett. **286**, L564 (1993).
[17] J. A. Barnard and J. J. Ehrhardt, J. Vac. Sci. Technol. A **8**, 4061 (1990).
[18] J. A. Barnard, J. J. Ehrhardt, H. Azzouzi, and M. Alnot, Surf. Sci. **211–212**, 740 (1989).
[19] S. Deckers, S. Offerhaus, F. H. P. M. Habraken, and W. F. van der Weg, Surf. Sci. **237**, 203 (1990).
[20] M. Romeo, J. Majerus, P. Legaré, N. J. Castellani, and D. B. Leroy, Surf. Sci. **238**, 163 (1990).
[21] N. J. Castellani and P. Legaré, J. Phys. Chem. **98**, 9606 (1994).
[22] N. J. Castellani, P. Legaré, P. Mikusik, S. Pick, and C. Demangeat, Surf. Sci. **307–309**, 927 (1994).
[23] P. Legaré, G. F. Cabeza, and N. J. Castellani, Surf. Rev. Lett. **5**, 581 (1998).
[24] P. Legaré, G. F. Cabeza, and N. J. Castellani, Surf. Sci. **441**, 461 (1999).
[25] W. Staiger, A. Michel, V. Pierron-Bohnes, N. Hermann, and M. C. Cadeville, J. Mater. Res. **12**, 161 (1997).
[26] O. Robach, C. Quiros, H. Isern, P. Steadman, K. F. Peters, and S. Ferrer, Phys. Rev. B **67**, 220405(R) (2003).
[27] S. Ferrer and F. Comin, Rev. Sci. Instrum. **66**, 1674 (1995).
[28] S. Ferrer, P. Fajardo, F. de Bergevin, J. Alvarez, X. Torrelles, H. A. van der Vegt, and V. H. Etgens, Phys. Rev. Lett. **77**, 747 (1996).
[29] S. Ferrer, J. Alvarez, E. Lundgren, X. Torrelles, P. Fajardo, and F. Boscherini, Phys. Rev. B **56**, 9848 (1997).
[30] J. Alvarez, E. Lundgren, X. Torrelles, H. Isern, K. F. Peters, P. Steadman, and S. Ferrer, Phys. Rev. B **60**, 10193 (1999).
[31] F. de Bergevin, M. Brunel, R. M. Galéra, and C. Vettier, Phys. Rev. B **46**, 10772 (1992).
[32] E. Vlieg, J. Appl. Crystallogr. **33**, 401 (2000).
[33] http://www.esrf.fr/computing/scientific/joint_projects/ANA-ROD/index.html.
[34] *International Tables for X-Ray Crystallography*, (Kynoch, Birmingham, England, 1974), Vol. IV, p. 71.
[35] O. Robach, G. Renaud, and A. Barbier, Phys. Rev. B **60**, 5858 (1999).
[36] F. Wilhelm, P. Poulopoulos, G. Ceballos, H. Wende, K. Baberschke, P. Srivastava, D. Benea, H. Ebert, M. Angelakaris, N. K. Flevaris, D. Niarchos, A. Rogalev, and N. B. Brookes, Phys. Rev. Lett. **85**, 413 (2000).
[37] http://www.esrf.fr/computing/scientific/joint_projects/ANA-ROD/index.html, ''Appendix to the Manual of the ROD program (experimental version): the Robach extension,'' Chap. II.4.
[38] For the (111) surface of a fcc crystal, the $H-K=3N\pm1$ rods are sensitive to the stacking (*ABC* or *ACB*) of the (111) planes, while the $H-K=3N$ rods are not. The reciprocal lattice of a crystal with the *ACB* stacking is the mirror image of the reciprocal lattice of a crystal with the *ABC* stacking. Here the mirror is the $L=0$ plane (which is a (111) plane).
[39] B. E. Warren, *X-ray Diffraction* (Dover, New York, 1990).
[40] H. Holloway, J. Appl. Phys. **40**, 4313 (1969).
[41] H. Bulou (private communication).
[42] L. A. Bruce, H. Jaeger, Philos. Mag. **36**, 1331 (1977).
[43] P. Bayle, Ph.D. thesis, University Joseph Fourier-Grenoble I, France, 1994.
[44] F. J. Lamelas, C. H. Lee, Hui He, W. Vavra, and Roy Clarke, Phys. Rev. B **40**, 5837 (1989).
[45] P. Boedeker, A. Abromeit, K. Broehl, P. Sonntag, N. Metoki, and H. Zabel, Phys. Rev. B **47**, 2353 (1993).
[46] K. Le Dang, P. Veillet, P. Beauvillain, C. Chappert, Hui He, F. J.

Lamelas, C. H. Lee, and R. Clarke, Phys. Rev. B **43**, 13 228 (1991).
[47] C. Rath, J. E. Prieto, S. Muller, R. Miranda, and K. Heinz, Phys. Rev. B **55**, 10 791 (1997).
[48] S. Muller, G. Kotska, T. Schafer, J. delaFiguera, J. E. Prieto, C. Ocal, R. Miranda, K. Heinz, and K. Muller, Surf. Sci. **352**, 46 (1996).
[49] C. E. Dahmani, Ph.D. thesis, Université Louis Pasteur (Strasbourg I), 1985.
[50] M. C. Cadeville, C. E. Dahmani, and F. Kern, J. Magn. Magn. Mater. **54–57**, 1055 (1986).
[51] Y. Gauthier, Surf. Rev. Lett. **3**, 1663 (1996).
[52] H. Ibach, Surf. Sci. Rep. **29**, 195 (1997).
[53] P. Gumbsch and M. S. Daw, Phys. Rev. B **44**, 3934 (1991).